International Journal of Biological Macromolecules 242 (2023) 124869

Contents lists available at ScienceDirect

International Journal of Biological Macromolecules

journal homepage: www.elsevier.com/locate/ijbiomac

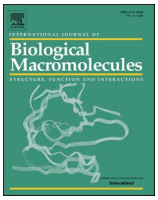

Nanocomposites of cellulose nanofibers incorporated with carvacrol via stabilizing octenyl succinic anhydride-modified ε-polylysine

Luana Amoroso [a], Kevin J. De France [a], Nico Kummer [a,b], Qun Ren [c], Gilberto Siqueira [a,*], Gustav Nyström [a,b,**]

[a] Laboratory for Cellulose & Wood Materials, Empa – Swiss Federal Laboratories for Materials Science and Technology, Überlandstrasse 129, 8600 DÜbendorf, Switzerland
[b] Department of Health Science and Technology, ETH Zürich, Schmelzbergstrasse 9, 8092 Zürich, Switzerland
[c] Laboratory for Biointerfaces, Empa – Swiss Federal Laboratories for Materials Science and Technology, Lerchenfeldstrasse 5, 9041 St. Gallen, Switzerland

ARTICLE INFO

Keywords:
Cellulose nanofibers
Epsilon-polylysine
Carvacrol
Composite
Active food packaging

ABSTRACT

Food packaging plays an extremely important role in the global food chain, allowing for products to be shipped across long distances without spoiling. However, there is an increased need to both reduce plastic waste caused by traditional single-use plastic packaging and improve the overall functionality of packaging materials to extend shelf-life even further. Herein, we investigate composite mixtures based on cellulose nanofibers and carvacrol via stabilizing octenyl-succinic anhydride-modified epsilon polylysine (MεPL-CNF) for active food packaging applications. The effects of epsilon polylysine (εPL) concentration and modification with octenyl-succinic anhydride (OSA) and carvacrol are evaluated with respect to composites morphology, mechanical, optical, antioxidant, and antimicrobial properties. We find that both increased εPL concentration and modification with OSA and carvacrol lead to films with increased antioxidant and antimicrobial properties, albeit at the expense of reduced mechanical performance. Importantly, when sprayed onto the surface of sliced apples, MεPL-CNF-mixtures are able to successfully delay/hinder enzymatic browning, suggesting the potential of such materials for a range of active food packaging applications.

1. Introduction

As the competition for shelf space has never been more intense, future packaging for the food industry must deliver a more compelling value proposition to the consumer [1]. Active packaging can be considered a natural progression in packaging innovation by performing some desired role in food preservation in addition to providing an inert barrier to external conditions [2]. Among available active packaging technologies, the incorporation of preservatives into packaging materials rather than adding them directly to the food is generally preferred, as the food remains chemically unchanged, while still serving a preservative function as part of its protective packaging [3,4].

The current interest in active packaging has focused on synthetic biodegradable polymers and natural polymers such as poly(lactic acid) (PLA), poly(hydroxy-alkanoates) (PHAs), thermoplastic starch, and cellulose nanofibers (CNF) [5]. Cellulose nanofibers are a promising bio-based nanomaterial that is a few nanometers in diameter and a few hundred to several thousand nanometers in length [6]. Owing to their biodegradability [7], good film-formability [8], remarkable mechanical and barrier properties [9–13], and their highly functionalized surface [14], CNF have become widely exploited as a polymeric matrix for the incorporation of active molecules in recent years [3,15]. Extensive research on the incorporation of active compounds into nanocellulose-based films and coatings has indeed highlighted their potential as an effective carrier for a wide range of antimicrobial and antioxidant agents [6,16–21].

Among various natural compounds, essential oils and their components have recently attracted widespread attention for active packaging applications[22]. Particularly, compounds with phenolic groups such as carvacrol (5-isopropyl-2-methylphenol) are highly effective as antimicrobial and antioxidant agents, thus they have been intensely studied for food preservation [23–26]. Carvacrol is well known for its antimicrobial activity against a broad spectrum of typical foodborne microorganisms, including *Botrytis cinerea*, *Escherichia coli* [27–30], *Staphylococcus aureus*

* Corresponding author.
** Correspondence to: Department of Health Science and Technology, ETH Zürich, Schmelzbergstrasse 9, 8092 Zürich, Switzerland.
E-mail addresses: gilberto.siqueira@empa.ch (G. Siqueira), gustav.nystroem@empa.ch (G. Nyström).

https://doi.org/10.1016/j.ijbiomac.2023.124869
Received 23 January 2023; Received in revised form 3 May 2023; Accepted 11 May 2023
Available online 16 May 2023

[30,31], *Candida albicans* [32], *Listeria innocua, Saccharomyces cerevisiae,* and *Aspergillus niger* [33]. Additionally, the antioxidant properties of carvacrol have been recognized for many years [34–36]. For these reasons, carvacrol has been incorporated into various substrates, including chitosan [37], starch [38], PLA [39], among others [40]. Although the highly hydrophobic nature of carvacrol may hinder its association with cellulose nanofibers, different methods can overcome this drawback, such as encapsulation and emulsification [41]. In a previous study, Lavoine et al. [42] developed a controlled release system based on paper coated with TEMPO-oxidized CNF and β-cyclodextrine (β-CD) in which the hydrophobic cavities were able to entrap the carvacrol by simple impregnation and drying treatment. Subsequently, the combined action of TEMPO-oxidized cellulose nanomaterials and β-CD to deliver carvacrol has been exploited by others [43,44]. To the best of our knowledge, no other strategies able to include carvacrol into nanocellulose matrices have been described in the literature. Despite this, recent studies are focusing on the incorporation of essential oils or their components into CNF or CNF-containing biopolymers [45–48].

Epsilon-Poly-L-Lysine (ε-polylysine or εPL) is a food-grade cationic homopolyamide of L-lysine produced by *Streptomyces albulus* [49]. Because of its excellent antimicrobial activity and heat stability, εPL has been used as a natural food preservative against a wide spectrum of Gram-positive and Gram-negative bacteria, yeasts, and molds [49–51]. Besides, hydrophobically modified ε-polylysine graft copolymers could be synthesized by reacting εPL with octenyl succinic anhydride (OSA) [52–54] that is widely used to yield amphiphilic hydrocolloids approved by the Food and Drug Administration (FDA) for food application purposes [55,56].

In the present study, a new method based on octenyl succinic anhydride-modified ε-polylysine (OSA-εPL) and surface-carboxylated (TEMPO-oxidized) CNF was developed as a potential strategy to entrap carvacrol for active packaging applications. Herein, the use of carvacrol and ε-polylysine was investigated in relation to their incorporation into CNF-based composites, placing particular emphasis on the resulting morphological, optical, mechanical, antioxidant, and antibacterial properties. A potential synergistic effect of combining carvacrol and ε-PL into TEMPO-oxidized CNF was assumed to be an advantage over previous methods as improved antimicrobial and antioxidant properties could be provided to the CNF matrix. As a proof of concept, the carvacrol-loaded εPL-CNF composites were also tested as spray coatings to hinder the enzymatic browning of sliced apples, demonstrating the potential of such materials for active food packaging.

Although the literature presents several studies using nanocellulose embedded in essential oils, no studies were found that reported the joint use of carvacrol and ε-PL to develop CNF-based active packaging.

2. Experimental

2.1. Materials

Never-dried elemental chlorine free cellulose fibers from bleached softwood pulp (*Picea abies* and Pinus app., chemical composition 81.3 % cellulose, 12.6 % hemicellulose, 0 % lignin and 0.3 % ash [57]) were obtained from Stendal GmbH (Berlin, Germany). 2,2,6,6-tetramethyl-1-piperidinyloxyl (TEMPO), 2,2-Diphenyl-1-picrylhydrazyl free radical (DPPH, ≥ 97.0 % purity), Deuterated chloroform ($CDCl_3$), Dimethyl Sulfoxide (DMSO), ethanol, and sodium hypochlorite solution (NaClO, 12–14 % chlorine) were obtained from VWR. Sodium hydroxide (NaOH), and 3-Aminopropyl triethoxysilane (APTES, 99 %) were obtained from Sigma-Aldrich. Sodium bromide (NaBr, ≥ 99 %) and sodium bicarbonate (NaHCO3, ≥ 99.7 %) were supplied by Carl Roth GmbH & Co. 2-octenylsuccinic anhydride (OSA, cis- and trans- mixture, > 95.0 %) and carvacrol (> 98.0 %) were purchased from Tokyo Chemical Industry Co. Ltd. Poly epsilon L-lysine (εPL, average MW 3500–4500 Da) was purchased from Carbosynth Limited. All chemicals were used as received without any further purification.

2.2. Synthesis of CNF via TEMPO-mediated oxidation

CNF were prepared via TEMPO-mediated oxidation as described in our previous work [58], whereby never dried cellulose pulp (33.3 wt% total solids) was dispersed in water to a final concentration of 2 wt%. TEMPO and NaBr were dissolved in water, and subsequently mixed with the cellulose pulp suspension at 0.1 and 1.0 mmol/g cellulose, respectively. The suspension pH was then adjusted to 10 by dropwise addition of 2 wt% NaOH. Finally, NaClO was added at 10 mmol/g cellulose, and the reaction proceeded under mild agitation at room temperature for 4–5 h. Following, the TEMPO-oxidized cellulose fibers were washed several times with distilled water, and subsequently ground using a Supermass Colloider (MKZA10-20 J CE Masuko Sangyo, Japan) at an applied energy of 9 kWh/kg. The CNF suspension was stored in a refrigerator at 4 °C until further use. TEMPO catalyzed oxidation produces individualized fibrils without significant aggregation and introduces functional carboxylate groups at the cellulose surface [59]. Morphological and chemical characteristics of the obtained CNF are available in the Supporting Information, Table S1.

2.3. Synthesis of OSA-εPL graft copolymer & loading of carvacrol (MεPL)

A 1:1 mixture of ε-polylysine and 2-octenyl succinic anhydride was reacted for 18 h in DMSO at 40 ± 5 °C to facilitate grafting, following the procedure of Yu et al. [53]. The reaction mixture was then dialyzed in 3500 Da molecular-weight-cut-off (MWCO) dialysis membrane against 95 % EtOH, 0.01 % $NaHCO_3$, and deionized water (twice sequentially) to remove any unreacted moieties or possible hydrolysates. The dialyzed mixture was then lyophilized to obtain the final OSA-εPL graft copolymers. Subsequently, carvacrol was loaded into the hydrophobic domain of self-assembled OSA-εPL graft copolymers, adapting a previously published method [54]. Briefly, 50 mg of OSA-εPL and 10 mg of carvacrol were dissolved in 10 mL DMSO and dialyzed for 6 cycles against distilled water (3500 Da MWCO). The mixture was then filtered through a 0.45 μm filter and lyophilized to obtain carvacrol-loaded OSA-εPL, herein referred to as MεPL.

2.4. Preparation of MεPL-CNF composite films

Based on our preliminary investigations, MεPL-CNF film forming mixtures were prepared by blending 0.5 wt% CNF aqueous suspension with MεPL to a final concentration of 0.10 wt% or 0.25 wt% (1:5 or 1:2 ratio with respect to CNF solid weight). Mixtures and subsequent films are denoted as MεPL010-CNF and MεPL025-CNF, respectively. In each case, MεPL was slowly added to the CNF aqueous suspension and vortex mixed until fully suspended. MεPL-CNF film forming mixtures were subsequently stirred for at least 1 h before further use to ensure homogeneity. For comparison, εPL-CNF mixtures were also prepared by simply dissolving pure εPL into CNF aqueous suspensions at the same concentrations as for MεPL (denoted as εPL010-CNF and εPL025-CNF). As above, the εPL-CNF mixtures were vortexed and subsequently stirred prior to further characterization/use. εPL-CNF and MεPL-CNF wet films were formed by vacuum filtration of the above-described formulations using a Buchner funnel and 0.65 μm filter (Durapore DVPP membrane filter, Merck Millipore Ltd.). Note that all films were formed from the same volume of ~0.5 wt% film-forming mixtures, yielding a basis weight of ~20 g/m^2 for each film. The wet films were subsequently hot pressed at 90 °C and 20 bar for 30 min. Dried films were stored at room temperature until characterization; as required, they were cut to size using a laser cutter (Nova24 60 W, Thunderlasers). CNF-only films were also fabricated using the same procedure for comparison.

2.5. Analyses of suspensions

The degree of substitution of α-amino groups of εPL by nucleophilic

reaction with OSA was calculated via ^{1}H NMR (Bruker 300 spectrometer operating at 300.13 MHz) in $CDCl_3$ following the description of Yu et al. [53]. FT-IR spectra of lyophilized OSA-εPL, MεPL, and their starting materials were recorded using a Bruker Tensor 27 FT-IR spectrometer in attenuated total reflectance (ATR) mode. Additionally, lyophilized film forming mixtures of εPL-CNF composites, with (MεPL010-CNF, MεPL025-CNF) and without carvacrol (εPL010-CNF, εPL025-CNF), were chemically analyzed by using FT-IR technique and compared with CNF-only material. All spectra were recorded between 4000 and 600 cm^{-1} with a resolution of 4 cm^{-1} and 32 scans per sample.

The aggregation behavior of composite and CNF-only mixtures was characterized via dynamic light scattering (DLS, 0.025 wt% in water), and zeta potential (0.25 wt% in 10 mM NaCl) using a ZetaSizer Nano ZS (Malvern), whereby all measurements were repeated in triplicate with results presented as the average ± standard deviation. The mean values of measured parameters were compared using Fisher's least significance difference (LSD) test, where the F-test was significant and with a significance level of $p \leq 0.05$. To this aim, a one-factor comparative experiment was performed, whose levels were represented by the film forming mixtures (CNF, εPL010-CNF, εPL025-CNF, MεPL010-CNF, MεPL025-CNF).

Particle morphology of the various composites was evaluated by high-resolution transmission electron microscopy (TEM, JEOL, JEM 2200fS) and atomic force microscopy (AFM, Bruker ICON3). Note that for AFM, samples were deposited on a freshly cleaved mica substrate modified with 0.05 % APTES at a sample concentration of ~2 g/L, and measured in tapping mode. TEM images were obtained after the samples (0.001 wt%) were deposited onto carbon-coated copper grids, stained by 1 wt% uranyl acetate.

2.6. Analyses of films

Scanning electron microscopy (SEM, FEI NanoSEM 230) was used to characterize the surface and cross-section microstructure of composite and CNF-only films.

Tensile testing was performed using a micromechanical testing device equipped with a 5 N load cell. Samples were strained at 1 μm/s until breakage to generate stress-strain curves. The Young's modulus was calculated from the initial linear portion of the curves, tensile strength was determined as the maximum stress achieved during testing, and toughness was calculated by numerically approximating the area under the stress-strain curve. Samples were tested in at least quintuplicate, with results presented as the average ± standard deviation. To differentiate CNF composites of each series from those of pristine CNF, all pairwise comparisons of means of measured mechanical properties were performed using Fisher's least significance difference (LSD) test, where the F-test was significant ($p \leq 0.05$).

Optical properties were evaluated via UV/Vis (UV3600 UV–vis NIR Spectrophotometer, Shimadzu). Film transparency was measured using an integrating sphere and $BaSO_4$ backplate, while film haze was calculated as the ratio of diffuse transmittance (no backplate) to film transparency.

Contact angle (CA) measurements were performed using the video-based optical contact angle measuring system OCA 20 (DataPhysics Instruments GmbH, Filderstadt, Germany). The contact angle of water in air at 20 °C and 65 % RH was determined by the sessile drop method by gently placed a 5 μL droplet on the film surface (5 × 20 mm strips). The drop shape was processed by an image analysis system and calculated with an accuracy of ±0.1°. The contact angle was taken as an average of at least twenty measurements, each being obtained as an average of the left and right contact angles of the water drop.

2.7. Assessment of active properties

DPPH free radical scavenging activity of all film forming mixtures was determined according to the procedure reported by Feng et al. [60] with slight modifications. In a test tube, 1.0 mL of film forming mixture was added to 4.0 mL of freshly prepared 0.1 mM DPPH ethanolic solution. The mixture was well shaken in a Vortex (3000 rpm), then stored in the dark for 30 min. The mixture was then centrifuged at 5000 rpm for 15 min and the supernatant was collected. The absorbance of the latter was read at 517 nm, using a Cary 1E UV–vis spectrophotometer (Varian). A blank comprising distilled water and ethanol, and a control containing only the DPPH solution were also run. DPPH radical scavenging activity was calculated as percent of inhibition (%) using the following formula:

$$\text{Radical scavenging activity}\% = \left(1 - \frac{A_i - \overline{A}_j}{A_c}\right) \times 100 \quad (1)$$

where A_i is the absorbance of the sample, $\bar{A}_j$ is the absorbance of the control, and A_c is the absorbance of the blank. All samples were assayed in at least triplicate for each condition.

The film's antimicrobial activity was tested against *Escherichia coli*, *Staphylococcus aureus* and *Candida albicans*. Films were cut into 10 mm diameter discs using a laser cutter as described above and were sterilized via exposure to UV light for 30 min under ambient conditions. Microbial cultures (*E. coli* DSMZ 1103, *S. aureus* ATCC 6538, and *C. albicans* ATCC 90028) were precultured in 5 mL of 30 % tryptic soy broth (TSB) plus 0.25 % glucose and incubated overnight at 37 °C at 40 rpm. Precultures were diluted to OD600 nm 0.001. Pre-cut films were then added to 1 mL of the diluted microbial culture and incubated for 2 h at 37 °C and 40 rpm. The films were finally placed on a PC-agar plate (Sigma-Aldrich 70152) which was incubated overnight at 37 °C prior to imaging. All samples were tested in at least triplicate for each condition.

2.8. Spraying test on apples

A suspension containing εPL-CNF or MεPL-CNF with a 1:5 or 1:2 ratio of active molecules with respect to CNF was prepared in order to form a 0.5 wt% solids mixture (as detailed above). This suspension, named as film forming mixture was sprayed onto the surface of locally purchased apples using an atomizing sprayer (Ultra-airbrush, Harder & Steenbeck Gmbh & Co. KG). Spraying only took place on the exposed surface of a half of apple (fruits were cut in half through the core immediately before spraying), while the remaining half was used as a control. The bare and coated half-apples were imaged with a digital camera for 1 h to evaluate the effects of the spray coating on fruit browning.

3. Results and discussion

In this study, the development of functional cellulose nanofibers incorporated with carvacrol via stabilizing OSA-modified ε-polylysine (MεPL-CNF) was investigated (Fig. 1). The interaction between the components was verified by ^{1}H NMR and FTIR-ATR spectroscopies. Firstly, ^{1}H NMR demonstrated the occurrence of the hydrophobic modification of α-amino groups of εPL by nucleophilic reaction with OSA, which served as preparation for the subsequent steps. The ^{1}H NMR spectra of OSA, εPL and OSA-εPL samples are shown in Fig. 2a. Compared to pure εPL, OSA-εPL graft copolymer showed additional peaks between 0.7 and 2.7 ppm attributed to the octenyl succinate group substitution [61]. Furthermore, the shift of the methine group of εPL from 3.8 to 4.0 ppm is indicative that some of the amine groups were acylated. The degree of substitution was found to be 23.9 %, which agrees well with previous findings using a similar OSA:εPL feed ratio [53].

OSA-εPL conjugation as well as the subsequent interaction with carvacrol to get MεPL was further investigated via FTIR (Fig. 2b). The absorption of all εPL-containing samples included contributions from the neutral amide NH and side chain amine NH_2 groups at 3400–3100 cm^{-1}, from charged (protonated) side chain NH_3^+ groups in the range

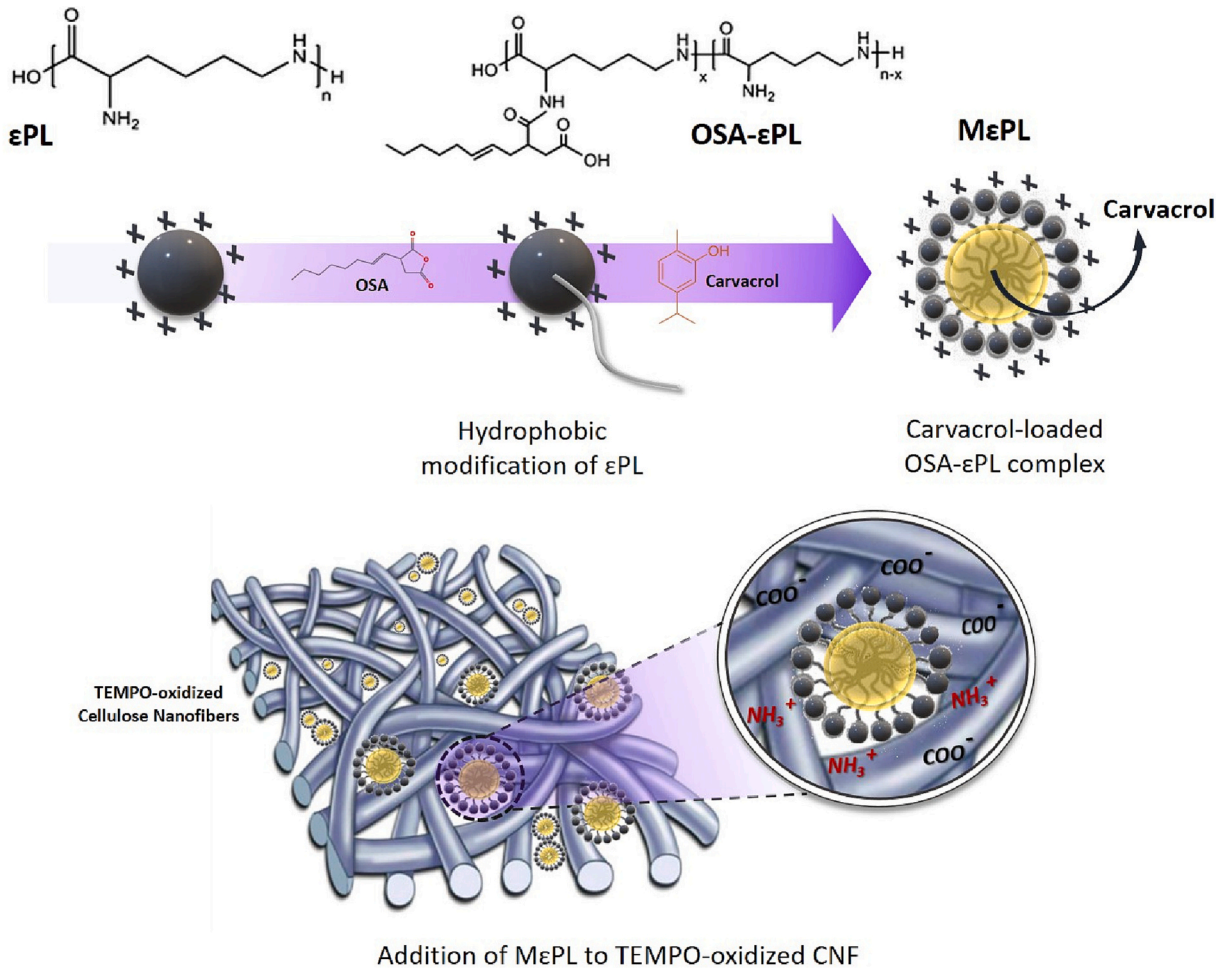

Fig. 1. Schematic representation of MεPL-CNF composite synthetic pathway.

3100–2500 cm^{-1} [62] along with from amide I, II and III groups between 1700 and 1200 cm^{-1} [63,64]. The pure εPL samples showed a broad absorbance peak centered around 3218 cm^{-1} identifying the stretching band of N—H groups. The position of this band shifted to around 3240 cm^{-1} and 3250 cm^{-1} in the OSA-εPL and MεPL spectra, respectively, suggesting the existence of hydrogen bonding between the N—H groups of εPL and the carbonyl (C=O) groups from OSA [53]. The weak band at approximately 3070–3050 cm^{-1} may be assigned to the overtone of the N—H stretching band (amide-II band) at 1560–1530 cm^{-1} [53,65]. The stretching modes of protonated -NH_3^+ side chain groups also fall in the range at ca. 3030–3050 cm^{-1} [62,66,67]. The intensity of this band was stronger upon hydrophobic substitution of εPL with OSA. Also, the two absorption bands of C—H stretching at 2925 and 2860 cm^{-1} were naturally more prominent than for pure εPL [53]. After the substitution, a redshift from 1662 to 1645 cm^{-1} occurred in the amide-I band, and a significant change was observed in the adsorption intensity at 1535 cm^{-1} in the amide-II band. The band at 1390 cm^{-1}, designated as methyl C—H bending, was significantly intensified in the OSA-εPL and MεPL spectra versus pure εPL. Although the absorption of MεPL was very similar to that of OSA-εPL, the addition of carvacrol led to the appearance of a new peak at 1014 cm^{-1} and a small shoulder at 950 cm^{-1} that might be traced back to the aromatic functionalities of the incorporated carvacrol [68–70].

Afterward, composite films were prepared from a mixture of negatively charged TEMPO-oxidized cellulose nanofibers (CNF) and the positively charged εPL or MεPL polypeptides. Successful composite formation was investigated via FTIR (Fig. 2c). Compared with pure CNF, broadening and shifting of the band at 1600 cm^{-1} combined with the appearance of a new shoulder at 1662 cm^{-1} occurred in all composite spectra, which may be attributed to the electrostatic interaction between COO^- of CNF and NH_3^+ of εPL and the C=O and –NH vibration bands in amide groups of the peptide ([64,71,72]; C. [73]). As expected, these distinctive bands were more prominent with an increase in εPL concentration in the composite films and upon the addition of carvacrol.

The addition of εPL or MεPL to the CNF matrix led to clear aggregation, as evidenced by the increase in size via DLS, and decrease in surface charge via zeta potential. As shown in Fig. 3a, the impact of this addition on z-average diameter and zeta potential was greater upon increasing the εPL (or MεPL) content. Note that, although some of the aggregates are too large to be reliably measured by DLS, the relative differences between samples are still assumed to be meaningful.

At 0.25 wt%, the partitioning of εPL at the surface of nanoparticles was such as to cause a rapid change in zeta potential from −42.7 mV to a positive value of 26.5 mV for εPL-CNF sample. This suggested a complete neutralization of the negatively charged colloidal surface of CNF. Nevertheless, MεPL caused less aggregation than εPL, and resulted in minor change in zeta potential. As the carvacrol molecules were physically entrapped into the hydrophobic domain of the self-assembled OSA–εPL block copolymers via the dialysis method, this might be due to the compact packing of the hydrophobic core of the polymer complex that acted reducing the overall surface charge density of MεPL as compared to the pure εPL. Consequently, the neutralization of negatively-charged nanofibers by εPL is attenuated to some extent, reducing aggregation and thereby suppressing DLS size increase. According to previous reports [53,54], the amphiphilic OSA-εPL copolymer can self-assemble to form a complex layer at the oil-water

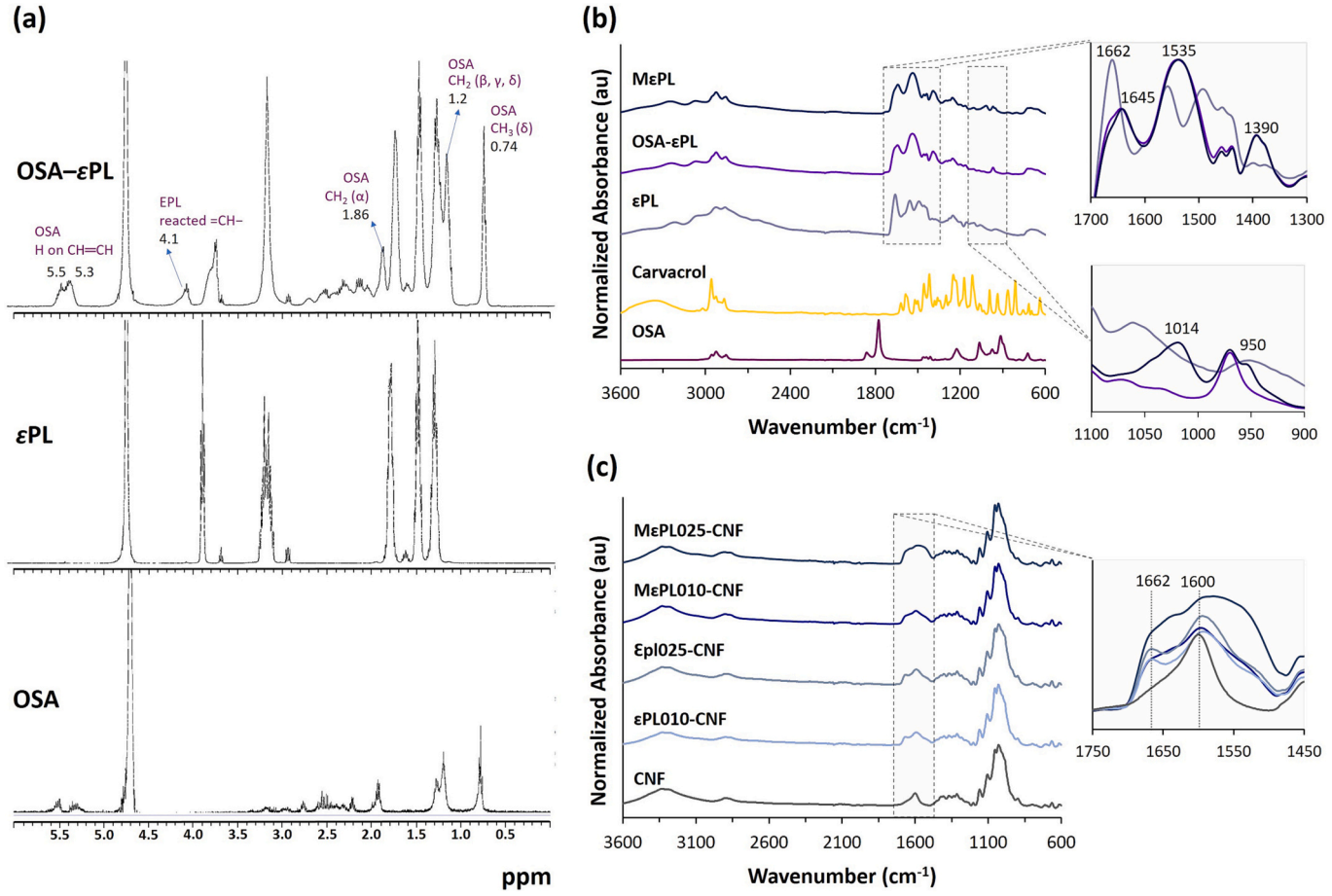

Fig. 2. Hydrophobic modification of εPL and loading of carvacrol via stabilizing OSA-modified εPL: (a) ^{1}H NMR spectra of OSA, εPL and OSA-εPL. (b) Normalized FTIR-ATR spectra of OSA-εPL, MεPL, and their pure components εPL, OSA and carvacrol; areas of interest are shown in the inset spectra. (c) Normalized FTIR-ATR spectra for CNF-only films, and εPL/MεPL-CNF composite films at varying εPL loading concentrations; the 1750–1450 cm^{-1} portion of the spectra is shown in the inset.

interface, which may serve as a microenvironment to water-insoluble bioactive compounds and thus increase their water solubility. It could be hypothesized that, as the organic solvent DMSO inside the dialysis bag was gradually replaced by water (non-solvent for the hydrophobic block), carvacrol was progressively loaded into self-associated polymeric complexes, having a hydrophobic core of OSA and a cationic shell of εPL (Fig. 1). Afterwards, the cationic shell of the complexes is expected to promote their electrostatic attraction to the negatively charged CNF, while the hydrophobic core still retained the poorly water-soluble carvacrol molecules. The presence of CNF nanoparticles in the vicinity of MεPL interfacial layer may additionally contribute to stabilizing the oil-water interface.

MεPL-CNF was morphologically analyzed and compared to εPL-CNF and CNF-only by TEM and AFM imaging. TEM evidenced a more uniform distribution of MεPL within the CNF matrix in comparison to pure εPL having the same loading concentration. In the TEM images (Fig. 3b), the CNF sample showed a network of randomly assembled nanofibers, while the composite samples (both containing 0.10 wt% of εPL or MεPL with respect to CNF weight) were also made up of nearly spherical nanoparticles (diameter ~30–40 nm), which adhered to the needle-like nanofibers. In MεPL010-CNF, these spherical nanoparticles appeared much well-dispersed throughout the surrounding nanofibers as compared with εPL010-CNF. As the loading concentration of εPL increased to 0.25 % by weight, more spheres of εPL (or MεPL) were adhered along the cellulose nanofibers, resulting in a partial concealment of the underlying nanofibers (Supporting Information, Fig. S1). Some globular particles clearly appeared also in the AFM image of MεPL010-CNF (Fig. 3c), while they were not visible in the composite without carvacrol. The large globular particles (50–100 nm) visible in Fig. 3c are attributable to carvacrol loaded OSA–εPL complexes that are agglomerated, while the smaller particles might be the same isolated complexes. At higher loadings (0.25 %), the entanglement and aggregation increased drastically, thereby making εPL025-CNF and MεPL025-CNF composites unable to be imaged via AFM.

The microstructure of the composite films was highly dependent on the loading concentration of εPL or MεPL as evidenced by SEM imaging. Cross-section micrographs of CNF-only films versus composite films at low and high εPL or MεPL loadings are shown in Fig. 4a (SEM images of the film surface are available in the Supporting Information, Fig. S2). At 0.10 wt% εPL or MεPL, a homogeneous, compact, and dense lamellar-like structure is observed, demonstrating a minor impact on film morphology compared with CNF only films. Conversely, the incorporation of 0.25 wt% εPL or MεPL led to an irregular, less compact morphology, with some large pores evidenced throughout the film cross-section (these could be formed from trapped air bubbles during the drying process, as mixtures with this high εPL/MεPL loading were qualitatively much more viscous) [74]. Furthermore, it is likely that the increase in εPL content reduces the cross-links between CNFs and the alignment of the nanofibers in the network, thereby increasing the spatial distance within the film matrix [73]. As a result, depending on the εPL or MεPL loading concentration the films showed different thicknesses of 9 ± 1, 11 ± 1, 24 ± 3, 14 ± 2, 30 ± 5 μm for CNF, εPL010-CNF, εPL025-CNF, MεPL010-CNF, MεPL025-CNF, respectively.

Film transparency was assessed by UV–vis spectroscopy (Fig. 5a),

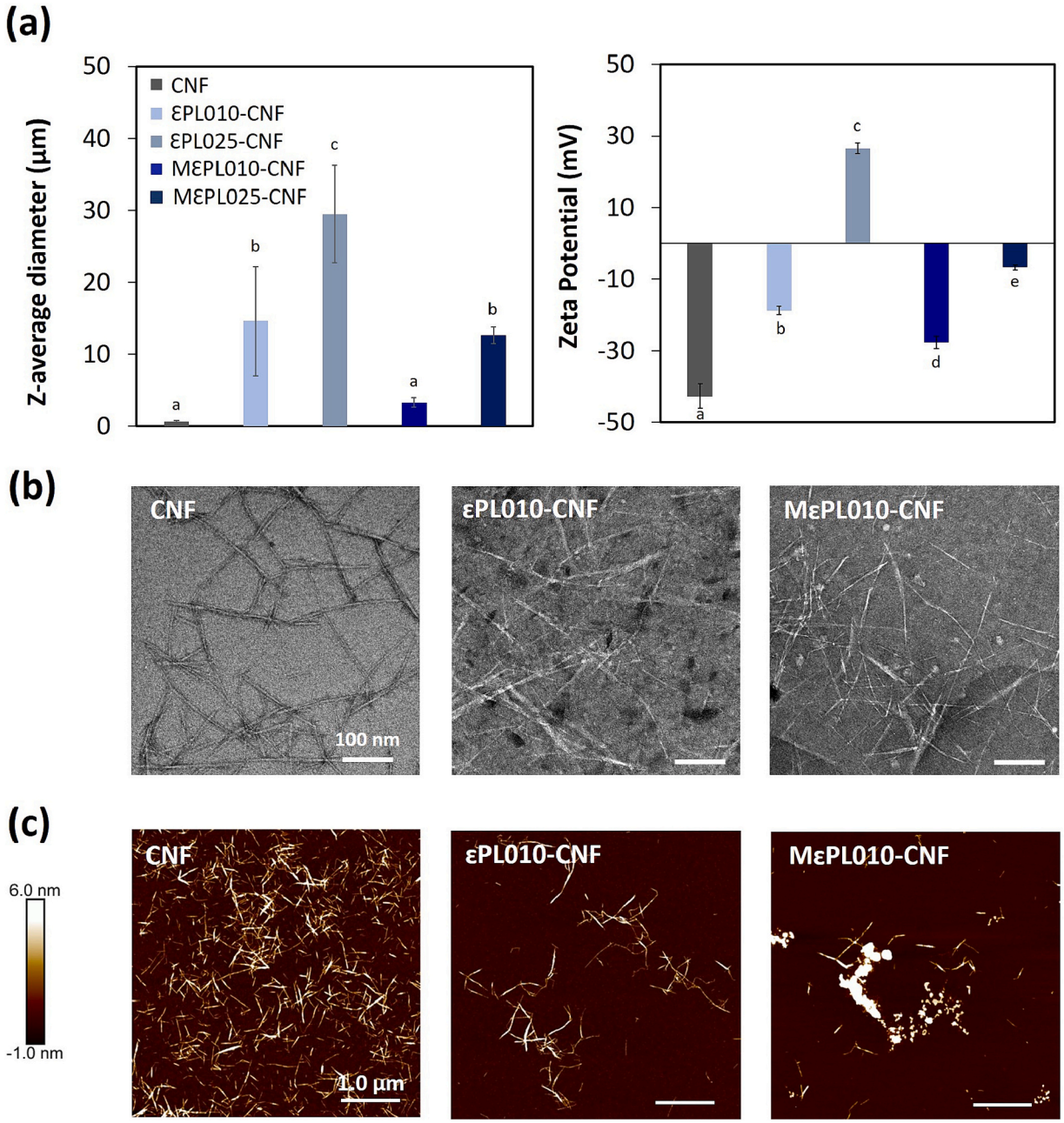

Fig. 3. (a) Comparison of the z-average diameter (as a qualitative measure of aggregate size) and the zeta potential (mean values with standard deviations) of εPL-CNF and MεPL-CNF composites. Same letter indicates statistical differences smaller than least significant difference (LSD) (not significant for $p \leq 0.05$). Microstructural characterization of composite mixtures: (b) TEM and (c) AFM micrographs for CNF-only, εPL010-CNF, and MεPL010-CNF suspensions.

whereby all films exhibited excellent transparency (> 80 %) in the visible range, regardless of εPL/MεPL loading. However, there were notable differences in film transparency in the UV range (< 400 nm), whereby the addition of MεPL led to a concentration-dependent absorbance of UV light. This is likely due to the high concentration of phenolic residues in carvacrol, which have a strong absorption in the UV region (maximum absorption at ~275 nm) [75,76]. These results are consistent with previous studies in which UV barrier properties have been observed via the incorporation of essential oils (or their components) into a film matrix [77–79]. This UV-blocking property could be extremely beneficial for food packaging applications, providing protection against oxidative deterioration (i.e., discoloration, loss of nutrients, off-flavors production) caused by UV radiation [77]. Notably, the incorporation of εPL and MεPL into CNF films did result in an increase in film haze (scattered light, Supporting Information, Table S2), which is likely due to increased film heterogeneity/porosity as observed via SEM.

Composite film mechanical properties were assessed via tensile testing (Fig. 5b, additional information in Table S2). For all samples, the stress-strain curves showed a relatively linear profile, indicative of purely elastic deformation and good interfacial adhesion/stress transfer during loading, typical for CNF-based films [80]. Compared to CNF only films, εPL010-CNF and MεPL010-CNF films showed an increase in tensile strength (from 59 MPa to 156 and 75 MPa, respectively, Fig. 5d), elongation at break (from 0.7 % to 1.3 and 1.4 %, respectively Fig. 5c), and toughness (from 0.22 MJ/m^3 to 1.17 and 0.62 MJ/m^3, respectively, Fig. 5f). This is likely due to the intercalation of εPL/MεPL between individual CNF, increasing the interfacial adhesion/inter-molecular interactions within the film [77]. This increase in the mechanical properties of CNF films following the addition of εPL is consistent with data from a previous work, in which amino-cellulose nanofiber films (ε-PL-

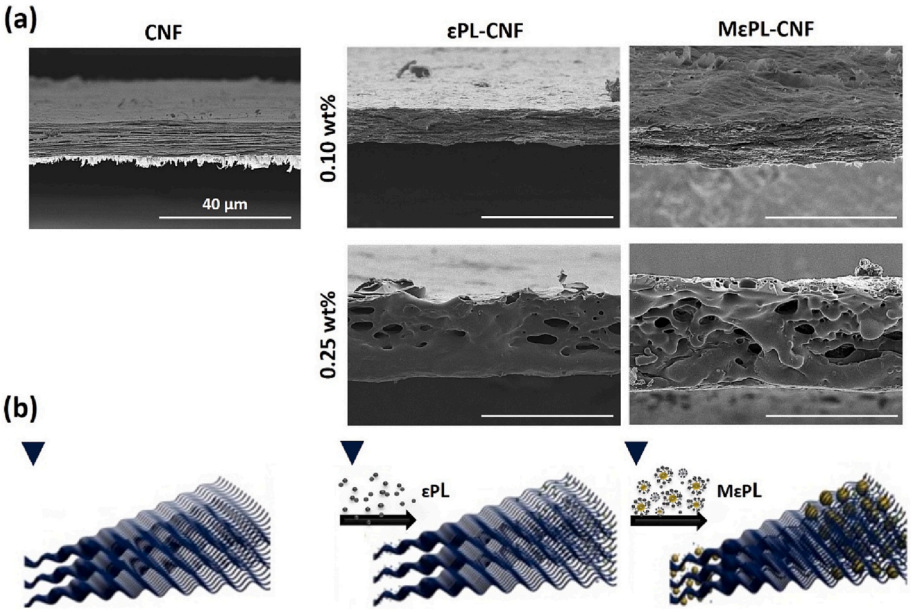

Fig. 4. (a) Scanning electron micrographs (magnification 5000×) of the cross-section of films made by CNF-only, εPL010-CNF, εPL025-CNF, MεPL010-CNF, and MεPL025-CNF. (b) Schematic illustration of films 3D network.

TOCNs) prepared by grafting ε-PL onto TEMPO-oxidized cellulose (TOCN) exhibited higher mechanical properties than TOCN films, attributing this behavior to the increase in hydrogen bonding due to the introduction of amine and amide bonds on polypeptide structures [81]. However, upon increased εPL/MεPL loading, mechanical properties decreased to values below even the CNF control. This systematic decline in mechanical performance is likely due to the increased heterogeneity/presence of void spaces in the film microstructure, as observed via SEM. This was also consistent with previous findings, where the tensile strength of composite nanocellulose-based films containing ε-PL was slightly increased from 36.2 MPa to 38.7 MPa than that of the control film and then decreased by further increasing the content of ε-PL [72].

The surface wettability of composite films was investigated by water contact angle (θ_w) as an indicator of the hydrophilic or hydrophobic character of a film surface [60]. As can be seen from contact angle measurements (Table S2 in Supporting Information), using the OSA-modification pathway rendered the MεPL-CNF composite films more hydrophobic compared to those produced with pure εPL at the same loading concentration. The θ_w values between 63° and 64° for CNF-only film, and both εPL-CNF composite films were indicative of rather hydrophilic surfaces. A significant increase ($\theta_w \sim 78$) in contact angle was observed for both MεPL films, indicating that the hydrophobicity of those composite films was greatly improved by the incorporation of hydrophobic OSA-εPL loaded with carvacrol. This is important for food packaging applications, as the increased hydrophobicity would lead to less diffusion of water into the film.

Active properties of the composite films were assessed in order to demonstrate the advantage of incorporating both preservatives, εPL and carvacrol, into CNF films. First, the antioxidant capacity of all film forming mixtures was determined as via DPPH radical scavenging activity, and the results are summarized in Fig. 6a-c. The effects of an antioxidant on DPPH are dependent to its ability to act as an electron donor (i.e., hydrogen-donor), being able to pair the odd electron of DPPH radical, thereby turning its color from purple to yellow [82]. From Fig. 6a, it is clearly seen that the strong absorption at 517 nm of DPPH from its odd electron was visibly reduced when the electron paired with a free radical scavenger in the film forming mixtures and, as expected, the degree of discoloration of DPPH was directly proportional to the percentage of electrons scavenged by the reaction system (see Fig. 6c). The antioxidant activity of neat CNF for DPPH, was equal to 59.2 ± 8.8 % (Fig. 6b),. Low levels (0.10 wt%) of εPL and MεPL led to percentages of radical removal very close to that of the CNF control, whereas a 19.4 % increase was recorded when 0.25 wt% εPL was loaded to CNF (albeit largely statistically insignificant). Nevertheless, among all cases, best radical inhibition, ~80 %, was achieved through the high-level incorporation of carvacrol via OSA-modified εPL (MεPL025), largely imputing this result to carvacrol molecules, which act as effective antioxidants. The antioxidant capacity of carvacrol has been proven to depend on the steric and electronic effect of its ring, besides the presence of the hydroxyl group which is capable of donating hydrogen atoms [77,83,84]. These findings are consistent with results of other authors, who incorporated carvacrol in chitosan [37], poly(lactic acid)/poly (ε-caprolactone) [69], starch [38], and flaxseed gum [85] films.

The antibacterial efficacy of εPL-CNF and MεPL-CNF composite films was qualitatively tested against Gram-positive *S. aureus*, Gram-negative *E. coli*, and fungal *C. albicans* (Fig. 6d and Fig. S3 of the Supporting Information). After exposure to εPL and MεPL, all three microbial strains showed clearly reduced growth on agar plates compared to those exposed to CNF-only films, demonstrating the antimicrobial activity of both εPL and MεPL. Furthermore, the concentration-dependent activity was observed against all three strains. Higher concentration of MεPL exhibited higher activity, whereas εPL displayed an opposite behavior, with the higher activity from the lower concentration. The latter might be due to the non-homogeneous dispersion of 0.25 wt% εPL within the CNF matrix. εPL has well-documented broad-spectrum antibacterial activity arising from its primary amine groups and positive charge [86,87]. This activity is typically more pronounced against Gram-positive bacteria, ([88]; [73]) as was observed here. Carvacrol is well known for its antimicrobial activity, whereby the presence of its phenolic residues can interact with the cell membrane of microorganisms causing loss of membrane structural integrity [38,77]. Furthermore, the hydroxyl groups on benzene rings of carvacrol play a crucial role in the antimicrobial activity of this phytochemical as they are capable of disrupting the equilibrium of inorganic ions and pH homeostasis in the cytoplasm of bacteria [38]. The poorer sensitivity of Gram-negative bacteria to carvacrol is due to differences in the structure and permeability of the bacterial cell membrane, such as the outer membrane that surrounds gram-negative microorganisms restricting the diffusion of hydrophobic compounds [33]. This behavior agrees with the results obtained herein. Against Candida, instead, carvacrol seems to

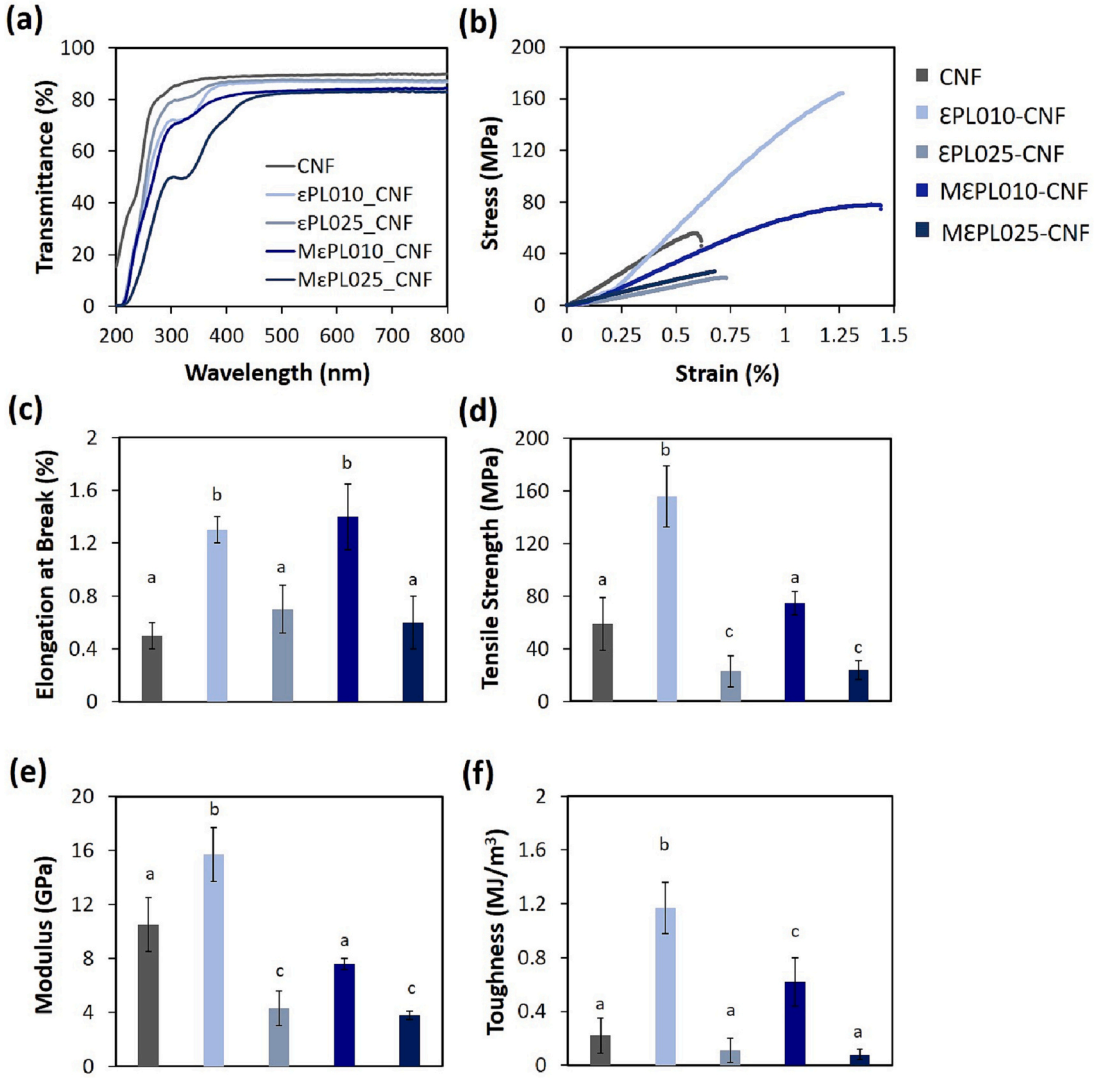

Fig. 5. Optical and mechanical characterization for CNF-only, εPL010-CNF, εPL025-CNF, MεPL010-CNF, and MεPL025-CNF films: (a) Representative UV–vis transmittance spectra, (b) representative stress-strain curves, (c) elongation at break, (d) tensile strength, (e) Young's modulus, and (f) Toughness. Error bars indicate the standard deviation of the mean of at least five replicates. Same letter indicates statistical differences smaller than least significant difference (LSD) (not significant for $p \leq 0.05$).

exert its antifungal activity by disrupting membrane integrity, and blocking ergosterol biosynthesis [89].

Finally, as a proof of concept for active food packaging, the effectiveness of εPL-CNF and MεPL-CNF spray coatings in preserving oxidation-sensitive foods was verified in locally purchased apples, which served as a model system. Importantly, in all cases, the spray coating was almost completely undetectable, as evidenced by the images taken directly after spraying (0 min) in comparison with the uncoated apples. This is crucial for practical application as active food packaging, as food products should retain their visual appeal. By comparing the images of control samples (uncoated sliced apples) with those of sprayed sliced apples (Fig. 7), it clearly appears that all film forming mixtures were effective in preventing enzymatic browning for up to 60 min post-spraying (Supporting Information, Video S1). Notably, at 60 min post-spraying, the control bare apples as well as those coated with CNF-only showed considerable enzymatic browning of the apple flesh. It can therefore be reasoned that the loading of active compounds, εPL and carvacrol, within CNF films are effective in delaying/inhibiting the oxidative reactions that lead to browning of the fruit surface.

4. Conclusion

In summary, composite mixtures of CNF with carvacrol loaded modified-εPL (MεPL) were prepared via simple electrostatic complexation, whereby the addition of increasing amounts of MεPL led to noticeable aggregation, as demonstrated via DLS, AFM, and TEM measurements, which hindered the optical transparency and mechanical properties of the films formed thereby. However, this high loading of MεPL also led to dual-functional CNF-based composites with significantly improved antioxidant activity (as measured via DPPH assay) and increased broad-spectrum antimicrobial activity against *S. aureus*, *E. coli*, and *C. albicans*, compared with either CNF or εPL alone. Importantly, MεPL-CNF composites were verified as sprayable active food packaging, whereby the enzymatic browning of sliced apples was drastically reduced after coating. Taken together, these results open the possibility to use such CNF-based composites for food packaging applications based solely on sustainable, natural materials. Nevertheless, additional studies may be required to further investigate key aspect of food packaging materials, including barrier properties, sensory evaluation, as well as to demonstrate compliance with the general safety requirements.

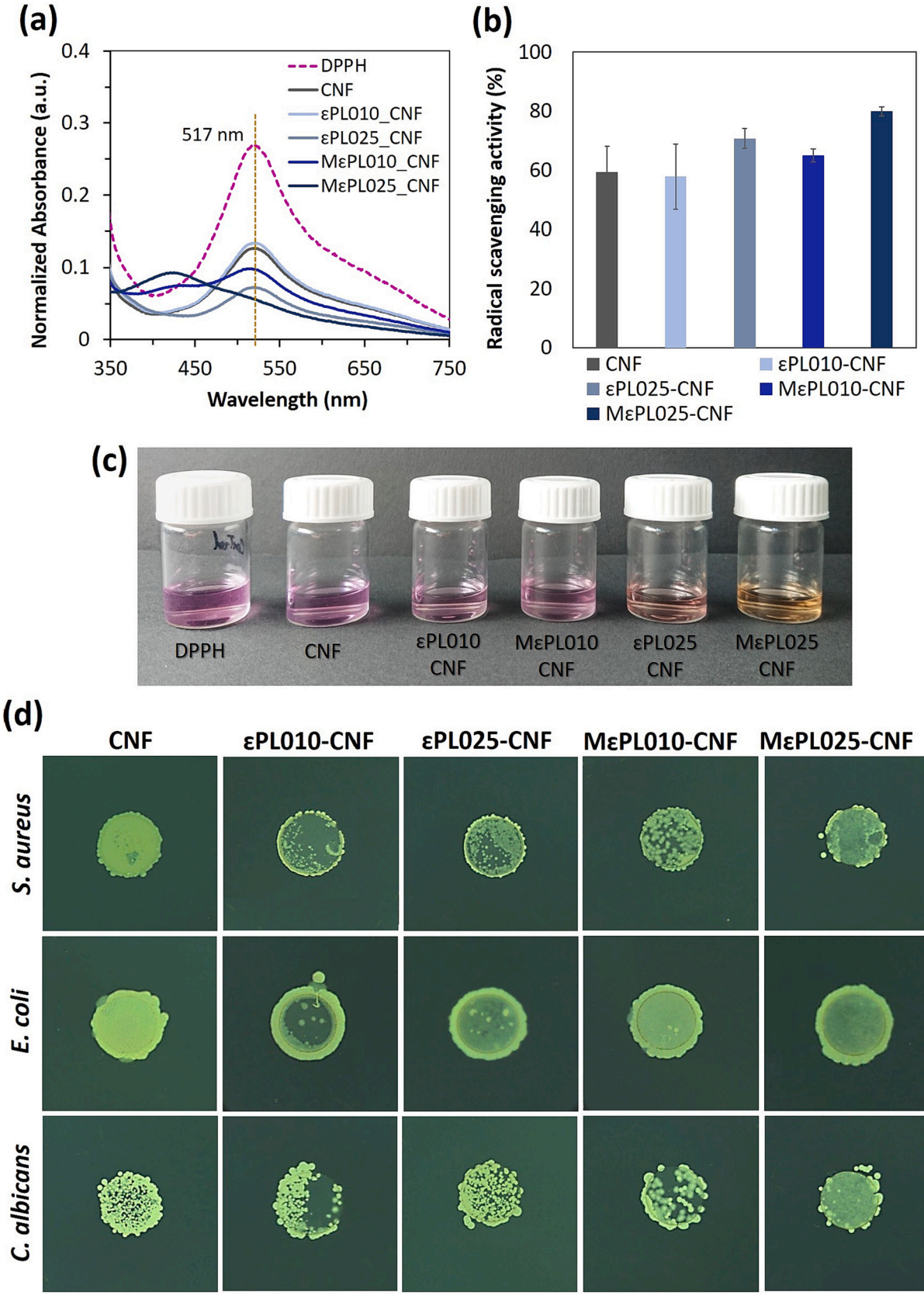

Fig. 6. Assessment of active properties of composite films: (a-b) evaluation of the radical scavenging activity of the film forming mixtures with varying εPL and MεPL content via DPPH assay. (c) Photographs of DPPH assay taken immediately after reading absorbance. (d) Antimicrobial activity of CNF-only film versus εPL−/MεPL−CNF composite films with varying loading concentration against *S. aureus*, *E. coli*, and *C. albicans*.

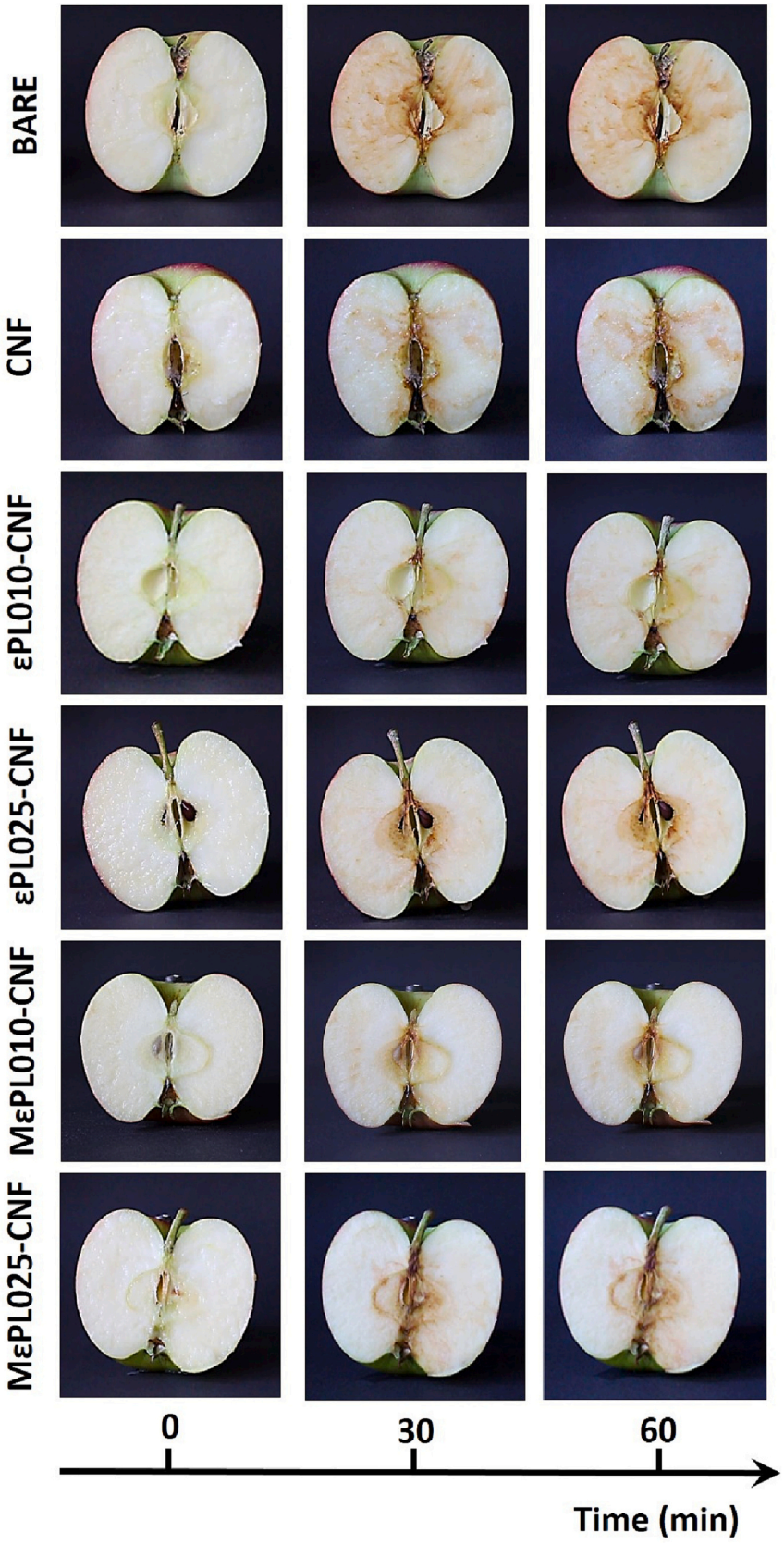

Fig. 7. Visual appearance of bare and sprayed sliced apples over 60 min post-spraying.

Additional TEM images of cellulose nanofibers containing εPL and MεPL at 0.25 wt% along with SEM images of films made thereof at high and low loading concentrations are provided. Images of the antimicrobial assay on agar plates are reported for three repeats of CNF-only films versus all εPL−/MεPL−CNF composite films. Data on mechanical properties, haze, and water contact angle of the composite CNF films are also provided. A video recording of bare and sprayed sliced apples over 60 min post-spraying is available. Supplementary data to this article can be found online at https://doi.org/10.1016/j.ijbiomac.2023.124869.

CRediT authorship contribution statement

Experiments were designed by L.A., K.D., G.S., and G.N., and were conducted by L.A. and K.D. NK performed the AFM measurements. QR was responsible for the antimicrobial assay. L.A. wrote the manuscript with input from all coauthors. All authors reviewed and commented on the manuscript.

Declaration of competing interest

The authors declare no competing financial interest.

Data availability

Data will be made available on request.

Acknowledgements

The authors thank Anja Huch for help with electron microscopy sample prep and imaging, and Flavia Zuber for antibacterial testing. KD gratefully acknowledges funding from the Natural Sciences and Engineering Research Council of Canada (NSERC) Postdoctoral Fellowship program. NK and GN also acknowledge funding from the Swiss National Science Foundation (Grant No. 200021_192225/1).

References

[1] J. Wyrwa, A. Barska, Innovations in the food packaging market: active packaging, Eur. Food Res. Technol. 243 (10) (2017) 1681–1692.
[2] K.B. Biji, C.N. Ravishankar, C.O. Mohan, T.K. Srinivasa Gopal, Smart packaging systems for food applications: a review, J. Food Sci. Technol. 52 (10) (2015) 6125–6135.
[3] A. Khan, T. Huq, R.A. Khan, B. Riedl, M. Lacroix, Nanocellulose-based composites and bioactive agents for food packaging, Crit. Rev. Food Sci. Nutr. 54 (2) (2014) 163–174.
[4] S. Yildirim, B. Röcker, M.K. Pettersen, J. Nilsen-Nygaard, Z. Ayhan, R. Rutkaite, T. Radusin, P. Suminska, B. Marcos, V. Coma, Active packaging applications for food, Compr. Rev. Food Sci. Food Saf. 17 (1) (2018) 165–199.
[5] N. Lin, J. Tang, A. Dufresne, M.K. Tam, Advanced Functional Materials From Nanopolysaccharides, Springer, Singapore, 2019.
[6] Y. Yang, H. Liu, M. Wu, J. Ma, P. Lu, Bio-based antimicrobial packaging from sugarcane bagasse nanocellulose/nisin hybrid films, Int. J. Biol. Macromol. 161 (2020) 627–635.
[7] M. Babaee, M. Jonoobi, Y. Hamzeh, A. Ashori, Biodegradability and mechanical properties of reinforced starch nanocomposites using cellulose nanofibers, Carbohydr. Polym. 132 (2015) 1–8.
[8] A. Dufresne, Nanocellulose: From Nature to High Performance Tailored Materials, 2nd ed., Walter de Gruyter GmbH & Co KG, Berlin, Boston, 2017.
[9] R.A. Carvalho, T.A. Santos, V.M. de Azevedo, P.H.C. Felix, M.V. Dias, S.V. Borges, Bio-nanocomposites for food packaging applications: effect of cellulose nanofibers on morphological, mechanical, optical and barrier properties, Polym. Int. 67 (4) (2018) 386–392.
[10] W. Deng, Y. Tang, J. Mao, Y. Zhou, T. Chen, X. Zhu, Cellulose nanofibril as a crosslinker to reinforce the sodium alginate/chitosan hydrogels, Int. J. Biol. Macromol. 189 (2021) 890–899.
[11] H. Fukuzumi, T. Saito, T. Iwata, Y. Kumamoto, A. Isogai, Transparent and high gas barrier films of cellulose nanofibers prepared by TEMPO-mediated oxidation, Biomacromolecules 10 (1) (2009) 162–165.
[12] K. Jin, Y. Tang, J. Liu, J. Wang, C. Ye, Nanofibrillated cellulose as coating agent for food packaging paper, Int. J. Biol. Macromol. 168 (2021) 331–338.
[13] B. Soni, E.B. Hassan, M.W. Schilling, B. Mahmoud, Transparent bionanocomposite films based on chitosan and TEMPO-oxidized cellulose nanofibers with enhanced mechanical and barrier properties, Carbohydr. Polym. 151 (Supplement C) (2016) 779–789.
[14] S. Sulaiman, M.N. Mokhtar, M.N. Naim, A.S. Baharuddin, A. Sulaiman, A review: potential usage of cellulose nanofibers (CNF) for enzyme immobilization via covalent interactions, Appl. Biochem. Biotechnol. 175 (4) (2015) 1817–1842.
[15] K. Kupnik, M. Primožič, V. Kokol, M. Leitgeb, Nanocellulose in drug delivery and antimicrobially active materials, Polymers 12 (12) (2020) 2825.
[16] A. Bahrami, R. Delshadi, S.M. Jafari, L. Williams, Nanoencapsulated nisin: an engineered natural antimicrobial system for the food industry, Trends Food Sci. Technol. 94 (2019) 20–31.
[17] N.A. El-Wakil, E.A. Hassan, R.E. Abou-Zeid, A. Dufresne, Development of wheat gluten/nanocellulose/titanium dioxide nanocomposites for active food packaging, Carbohydr. Polym. 124 (2015) 337–346.
[18] A. Jebali, S. Hekmatimoghaddam, A. Behzadi, I. Rezapor, B.H. Mohammadi, T. Jasemizad, S.A. Yasini, M. Javadzadeh, A. Amiri, M. Soltani, Z. Rezaei, N. Sedighi, M. Seyfi, M. Rezaei, M. Sayadi, Antimicrobial activity of nanocellulose conjugated with allicin and lysozyme, Cellulose 20 (6) (2013) 2897–2907.
[19] C. Nerín, 16 - antioxidant active food packaging and antioxidant edible films, in: E. A. Decker, R.J. Elias, D. Julian McClements (Eds.), Oxidation in Foods And Beverages And Antioxidant Applications, Woodhead Publishing, 2010, pp. 496–515.
[20] F.A.G.S. Silva, F. Dourado, M. Gama, F. Poças, Nanocellulose bio-based composites for food packaging, Nanomaterials 10 (10) (2020) 2041.
[21] Y.-H. Tsai, Y.-N. Yang, Y.-C. Ho, M.-L. Tsai, F.-L. Mi, Drug release and antioxidant/antibacterial activities of silymarin-zein nanoparticle/bacterial cellulose nanofiber composite films, Carbohydr. Polym. 180 (2018) 286–296.
[22] A. Rehman, S.M. Jafari, R.M. Aadil, E. Assadpour, M.A. Randhawa, S. Mahmood, Development of active food packaging via incorporation of biopolymeric nanocarriers containing essential oils, Trends Food Sci. Technol. 101 (2020) 106–121.
[23] S. Burt, Essential oils: their antibacterial properties and potential applications in foods—a review, Int. J. Food Microbiol. 94 (3) (2004) 223–253.
[24] M.H. Hosseini, S.H. Razavi, M.A. Mousavi, Antimicrobial, physical and mechanical properties of chitosan-based films incorporated with thyme, clove and cinnamon essential oils, J.Food Process.Preserv. 33 (6) (2009) 727–743.
[25] G. Nieto, A review on applications and uses of thymus in the food industry, Plants 9 (8) (2020) 961.
[26] F. Shahidi, P. Ambigaipalan, Phenolics and polyphenolics in foods, beverages and spices: antioxidant activity and health effects – a review, J. Funct. Foods 18 (2015) 820–897.
[27] A. Ben Arfa, L. Preziosi-Belloy, P. Chalier, N. Gontard, Antimicrobial paper based on a soy protein isolate or modified starch coating including carvacrol and cinnamaldehyde, J. Agric. Food Chem. 55 (6) (2007) 2155–2162.
[28] W.-X. Du, C.W. Olsen, R.J. Avena-Bustillos, T.H. McHugh, C.E. Levin, M. Friedman, Storage stability and antibacterial activity against Escherichia coli O157:H7 of carvacrol in edible apple films made by two different casting methods, J. Agric. Food Chem. 56 (9) (2008) 3082–3088.
[29] E. Mascheroni, V. Guillard, E. Gastaldi, N. Gontard, P. Chalier, Anti-microbial effectiveness of relative humidity-controlled carvacrol release from wheat gluten/montmorillonite coated papers, Food Control 22 (10) (2011) 1582–1591.
[30] S. Tunç, O. Duman, Preparation of active antimicrobial methyl cellulose/carvacrol/montmorillonite nanocomposite films and investigation of carvacrol release, LWT Food Sci. Technol. 44 (2) (2011) 465–472.
[31] M. Ramos, A. Jiménez, M. Peltzer, M.C. Garrigós, Characterization and antimicrobial activity studies of polypropylene films with carvacrol and thymol for active packaging, J. Food Eng. 109 (3) (2012) 513–519.
[32] R.J.W. Lambert, P.N. Skandamis, P.J. Coote, G.-J.E. Nychas, A study of the minimum inhibitory concentration and mode of action of oregano essential oil, thymol and carvacrol, J. Appl. Microbiol. 91 (3) (2001) 453–462.
[33] A. Guarda, J.F. Rubilar, J. Miltz, M.J. Galotto, The antimicrobial activity of microencapsulated thymol and carvacrol, Int. J. Food Microbiol. 146 (2) (2011) 144–150.
[34] R. Aeschbach, J. Löliger, B.C. Scott, A. Murcia, J. Butler, B. Halliwell, O.I. Aruoma, Antioxidant actions of thymol, carvacrol, 6-gingerol, zingerone and hydroxytyrosol, Food Chem. Toxicol. 32 (1) (1994) 31–36.
[35] T. Kulisic, A. Radonic, V. Katalinic, M. Milos, Use of different methods for testing antioxidative activity of oregano essential oil, Food Chem. 85 (4) (2004) 633–640.
[36] M. Ramos, A. Beltrán, M. Peltzer, A.J.M. Valente, M.d.C. Garrigós, Release and antioxidant activity of carvacrol and thymol from polypropylene active packaging films, LWT Food Sci. Technol. 58 (2) (2014) 470–477.
[37] M.A. López-Mata, S. Ruiz-Cruz, N.P. Silva-Beltrán, J.D.J. Ornelas-Paz, P. B. Zamudio-Flores, S.E. Burruel-Ibarra, Physicochemical, antimicrobial and antioxidant properties of chitosan films incorporated with carvacrol, Molecules 18 (11) (2013) 13735–13753.
[38] L.M. Fonseca, C.E.d.S. Cruxen, G.P. Bruni, Â.M. Fiorentini, E.d.R. Zavareze, L.-T. Lim, A.R.G. Dias, Development of antimicrobial and antioxidant electrospun soluble potato starch nanofibers loaded with carvacrol, Int. J. Biol. Macromol. 139 (2019) 1182–1190.
[39] Y. Qin, W. Li, D. Liu, M. Yuan, L. Li, Development of active packaging film made from poly (lactic acid) incorporated essential oil, Prog.Org.Coat. 103 (2017) 76–82.
[40] P. Klinmalai, A. Srisa, Y. Laorenza, W. Katekhong, N. Harnkarnsujarit, Antifungal and plasticization effects of carvacrol in biodegradable poly(lactic acid) and poly (butylene adipate terephthalate) blend films for bakery packaging, LWT 152 (2021), 112356.
[41] M. Ben Jemaa, H. Falleh, K. Riadh, Encapsulation of natural bioactive compounds: nanoemulsion formulation to enhance essential oils activities, 2019.

[42] N. Lavoine, C. Givord, N. Tabary, I. Desloges, B. Martel, J. Bras, Elaboration of a new antibacterial bio-nano-material for food-packaging by synergistic action of cyclodextrin and microfibrillated cellulose, Innovative Food Sci. Emerg. Technol. 26 (2014) 330–340.
[43] D.O. Castro, N. Tabary, B. Martel, A. Gandini, N. Belgacem, J. Bras, Effect of different carboxylic acids in cyclodextrin functionalization of cellulose nanocrystals for prolonged release of carvacrol, Mater. Sci. Eng. C 69 (2016) 1018–1025.
[44] D.O. de Castro, N. Tabary, B. Martel, A. Gandini, N. Belgacem, J. Bras, Controlled release of carvacrol and curcumin: bio-based food packaging by synergism action of TEMPO-oxidized cellulose nanocrystals and cyclodextrin, Cellulose 25 (2) (2018) 1249–1263.
[45] Y. Montero, A.G. Souza, É.R. Oliveira, D.d.S. Rosa, Nanocellulose functionalized with cinnamon essential oil: a potential application in active biodegradable packaging for strawberry, Sustain. Mater. Technol. 29 (2021), e00289.
[46] E.L.P.d. Silva, T.C.d. Carvalho, R.A. Ayub, M.C. Almeida, Nanocellulose coating associated with lemongrass essential oil at postharvest of blackberry fruits, 2019.
[47] M.P. Silveira, H.C. Silva, I.C. Pimentel, C.G. Poitevin, A.K. da Costa Stuart, D. Carpiné, L.M. de Matos Jorge, R.M.M. Jorge, Development of active cassava starch cellulose nanofiber-based films incorporated with natural antimicrobial tea tree essential oil, J. Appl. Polym. Sci. 137 (21) (2020) 48726.
[48] A.G.d. Souza, R.R. Ferreira, E.S.F. Aguilar, L. Zanata, D.d.S. Rosa, Cinnamon essential oil nanocellulose-based pickering emulsions: processing parameters effect on their formation, stabilization, and antimicrobial activity, Polysaccharides 2 (3) (2021) 608–625.
[49] I.-L. Shih, M.-H. Shen, Y.-T. Van, Microbial synthesis of poly(ε-lysine) and its various applications, Bioresour. Technol. 97 (9) (2006) 1148–1159.
[50] L. Bi, L. Yang, A.K. Bhunia, Y. Yao, Emulsion stabilized with phytoglycogen octenyl succinate prolongs the antimicrobial efficacy of ε-poly-l-lysine against Escherichia coli O157:H7, LWT 70 (2016) 245–251.
[51] Q. Tang, D. Pan, Y. Sun, J. Cao, Y. Guo, Preparation, characterization and antimicrobial activity of sodium alginate nanobiocomposite films incorporated with E-polylysine and cellulose nanocrystals, J.Food Process.Preserv. 41 (5) (2017), e13120.
[52] S.L. Scheffler, X. Wang, L. Huang, F. San-Martin Gonzalez, Y. Yao, Phytoglycogen octenyl succinate, an amphiphilic carbohydrate nanoparticle, and ε-polylysine to improve lipid oxidative stability of emulsions, J. Agric. Food Chem. 58 (1) (2010) 660–667.
[53] H. Yu, Y. Huang, Q. Huang, Synthesis and characterization of novel antimicrobial emulsifiers from ε-polylysine, J. Agric. Food Chem. 58 (2) (2010) 1290–1295.
[54] H. Yu, J. Li, K. Shi, Q. Huang, Structure of modified ε-polylysine micelles and their application in improving cellular antioxidant activity of curcuminoids, Food Funct. 2 (7) (2011) 373–380.
[55] H. Namazi, F. Fathi, A. Dadkhah, Hydrophobically modified starch using long-chain fatty acids for preparation of nanosized starch particles, Sci.Iran. 18 (3) (2011) 439–445.
[56] M. Omar-Aziz, M.S. Yarmand, F. Khodaiyan, M. Mousavi, M. Gharaghani, J. F. Kennedy, S.S. Hosseini, Chemical modification of pullulan exopolysaccharide by octenyl succinic anhydride: optimization, physicochemical, structural and functional properties, Int. J. Biol. Macromol. 164 (2020) 3485–3495.
[57] S. Josset, P. Orsolini, G. Siqueira, A. Tejado, P. Tingaut, T. Zimmermann, Energy consumption of the nanofibrillation of bleached pulp, wheat straw and recycled newspaper through a grinding process, Nordic PulpPap.Res.J. 29 (1) (2014) 167–175.
[58] D. França, G. Siqueira, G. Nyström, F. Clemens, C.F. Souza, R. Faez, Charged-cellulose nanofibrils as a nutrient carrier in biodegradable polymers for enhanced efficiency fertilizers, Carbohydr. Polym. 296 (2022), 119934.
[59] A. Isogai, T. Saito, H. Fukuzumi, TEMPO-oxidized cellulose nanofibers, Nanoscale 3 (1) (2011) 71–85.
[60] Z. Feng, G. Wu, C. Liu, D. Li, B. Jiang, X. Zhang, Edible coating based on whey protein isolate nanofibrils for antioxidation and inhibition of product browning, Food Hydrocoll. 79 (2018) 179–188.
[61] F. Tong, L. Deng, R. Sun, G. Zhong, Effect of octenyl succinic anhydride starch ester by semi-dry method with vacuum-microwave assistant, Int. J. Biol. Macromol. 141 (2019) 1128–1136.
[62] M. Rozenberg, G. Shoham, FTIR spectra of solid poly-l-lysine in the stretching NH mode range, Biophys. Chem. 125 (1) (2007) 166–171.
[63] L. Lin, L. Xue, S. Duraiarasan, C. Haiying, Preparation of ε-polylysine/chitosan nanofibers for food packaging against salmonella on chicken, Food Packag. Shelf Life 17 (2018) 134–141.
[64] F. Liu, Y. Liu, Z. Sun, D. Wang, H. Wu, L. Du, D. Wang, Preparation and antibacterial properties of ε-polylysine-containing gelatin/chitosan nanofiber films, Int. J. Biol. Macromol. 164 (2020) 3376–3387.
[65] G. Amariei, V. Kokol, V. Vivod, K. Boltes, P. Letón, R. Rosal, Biocompatible antimicrobial electrospun nanofibers functionalized with ε-poly-l-lysine, Int. J. Pharm. 553 (1) (2018) 141–148.
[66] S. Jia, B. Fan, Y. Dai, G. Wang, P. Peng, Y. Jia, Fractionation and characterization of ε-poly-l-lysine from Streptomyces albulus CGMCC 1986, Food Sci. Biotechnol. 19 (2) (2010) 361–366.
[67] R.A. Sequeira, N. Singh, M.M. Pereira, N.A. Chudasama, S. Bhattacharya, M. Sharma, D. Mondal, K. Prasad, High concentration solubility and stability of ε-poly-l-lysine in an ammonium-based ionic liquid: a suitable media for polypeptide packaging and biomaterial preparation, Int. J. Biol. Macromol. 120 (2018) 378–384.
[68] D.R. Chambre, C. Moisa, A. Lupitu, L. Copolovici, G. Pop, D.-M. Copolovici, Chemical composition, antioxidant capacity, and thermal behavior of Satureja hortensis essential oil, Sci. Rep. 10 (1) (2020) 21322.
[69] I. Lukic, J. Vulic, J. Ivanovic, Antioxidant activity of PLA/PCL films loaded with thymol and/or carvacrol using scCO2 for active food packaging, Food Packag. Shelf Life 26 (2020), 100578.
[70] A.C.S. Valderrama, G.C.R. De, Traceability of active compounds of essential oils in antimicrobial food packaging using a chemometric method by ATR-FTIR, Am. J. Anal. Chem. 8 (11) (2017) 726.
[71] C. Gao, T. Yan, J. Du, F. He, H. Luo, Y. Wan, Introduction of broad spectrum antibacterial properties to bacterial cellulose nanofibers via immobilising ε-polylysine nanocoatings, Food Hydrocoll. 36 (2014) 204–211.
[72] F. Wahid, F.P. Wang, Y.Y. Xie, L.Q. Chu, S.R. Jia, Y.X. Duan, L. Zhang, C. Zhong, Reusable ternary PVA films containing bacterial cellulose fibers and epsilon-polylysine with improved mechanical and antibacterial properties, Colloids Surf. B: Biointerfaces 183 (2019), 110486.
[73] C. Wu, J. Sun, Y. Lu, T. Wu, J. Pang, Y. Hu, In situ self-assembly chitosan/ε-polylysine bionanocomposite film with enhanced antimicrobial properties for food packaging, Int. J. Biol. Macromol. 132 (2019) 385–392.
[74] E. Jahed, M.A. Khaledabad, H. Almasi, R. Hasanzadeh, Physicochemical properties of Carum copticum essential oil loaded chitosan films containing organic nanoreinforcements, Carbohydr. Polym. 164 (2017) 325–338.
[75] L. Keawchaoon, R. Yoksan, Preparation, characterization and in vitro release study of carvacrol-loaded chitosan nanoparticles, Colloids Surf. B: Biointerfaces 84 (1) (2011) 163–171.
[76] I. Partheniadis, P. Karakasidou, S. Vergkizi, I. Nikolakakis, Spectroscopic examination and release of microencapsulated oregano essential oil, ADMET and DMPK 5 (4) (2017) 224–233.
[77] Ł. Łopusiewicz, P. Kwiatkowski, E. Drozłowska, P. Trocer, M. Kostek, M. Śliwiński, M. Polak-Śliwińska, E. Kowalczyk, M. Sienkiewicz, Preparation and characterization of carboxymethyl cellulose-based bioactive composite films modified with fungal melanin and carvacrol, Polymers 13 (4) (2021) 499.
[78] S. Sharma, S. Barkauskaite, B. Duffy, A.K. Jaiswal, S. Jaiswal, Characterization and antimicrobial activity of biodegradable active packaging enriched with clove and thyme essential oil for food packaging application, Foods 9 (8) (2020) 1117.
[79] J. Wu, X. Sun, X. Guo, S. Ge, Q. Zhang, Physicochemical properties, antimicrobial activity and oil release of fish gelatin films incorporated with cinnamon essential oil, Aquac.Fish. 2 (4) (2017) 185–192.
[80] J. Desmaisons, E. Boutonnet, M. Rueff, A. Dufresne, J. Bras, A new quality index for benchmarking of different cellulose nanofibrils, Carbohydr. Polym. 174 (2017) 318–329.
[81] S. Zhang, H. Chen, Z. Shi, Y. Liu, L. Liu, J. Yu, Y. Fan, Preparation of amino cellulose nanofiber via ε-poly-L-lysine grafting with enhanced mechanical, anti-microbial and food preservation performance, Ind. Crop. Prod. 194 (2023), 116288.
[82] W. Ge, S. Cao, F. Shen, Y. Wang, J. Ren, X. Wang, Rapid self-healing, stretchable, moldable, antioxidant and antibacterial tannic acid-cellulose nanofibril composite hydrogels, Carbohydr. Polym. 224 (2019), 115147.
[83] S. Fang, Q. Zhou, Y. Hu, F. Liu, J. Mei, J. Xie, Antimicrobial carvacrol incorporated in flaxseed gum-sodium alginate active films to improve the quality attributes of Chinese Sea bass (Lateolabrax maculatus) during cold storage, Molecules 24 (18) (2019) 3292.
[84] K. Lei, X. Wang, X. Li, L. Wang, The innovative fabrication and applications of carvacrol nanoemulsions, carboxymethyl chitosan microgels and their composite films, Colloids Surf. B: Biointerfaces 175 (2019) 688–696.
[85] S. Fang, W. Qiu, J. Mei, J. Xie, Effect of sonication on the properties of flaxseed gum films incorporated with carvacrol, Int. J. Mol. Sci. 21 (5) (2020) 1637.
[86] M. Hyldgaard, T. Mygind, B.S. Vad, M. Stenvang, D.E. Otzen, R.L. Meyer, The antimicrobial mechanism of action of epsilon-poly-l-lysine, Appl. Environ. Microbiol. 80 (24) (2014) 7758–7770.
[87] Z. Tan, Y. Shi, B. Xing, Y. Hou, J. Cui, S. Jia, The antimicrobial effects and mechanism of ε-poly-lysine against Staphylococcus aureus, Bioresour.Bioprocess. 6 (1) (2019) 11.
[88] J. Švedienė, V. Novickij, R. Žalnėravičius, V. Raudonienė, S. Markovskaja, J. Novickij, A. Paškevičius, Antimicrobial activity of L-lysine and poly-L-lysine with pulsed electric fields, Appl. Sci. 11 (6) (2021) 2708.
[89] I.O. Lima, F.d.O. Pereira, W.A.d. Oliveira, E.d.O. Lima, E.A. Menezes, F.A. Cunha, M.d.F.F.M. Diniz, Antifungal activity and mode of action of carvacrol against Candida albicans strains, J. Essent. Oil Res. 25 (2) (2013) 138–142.